






## Article

# Self-Standing Adsorbent Composites of Waste-Derived Biochar and Reduced Graphene Oxide for Water Decontamination

Anna Dotti <sup>1</sup> , Marianna Guagliano <sup>1,\*</sup> , Vittorio Ferretti di Castelferretto <sup>1,2</sup>, Roberto Scotti <sup>3</sup>, Simone Pedrazzi <sup>4</sup> , Marco Puglia <sup>4</sup> , Romano V. A. Orrù <sup>2</sup>, Cinzia Cristiani <sup>1</sup> , Elisabetta Finocchio <sup>5</sup>, Andrea Basso Peressut <sup>1</sup>  and Saverio Latorrata <sup>1,\*</sup> 

<sup>1</sup> Department of Chemistry, Materials and Chemical Engineering “Giulio Natta”, Politecnico di Milano, Piazza Leonardo Da Vinci 32, 20133 Milano, Italy; anna.dotti@polimi.it (A.D.); vittorioferretti@gmail.com (V.F.d.C.); cinzia.cristiani@polimi.it (C.C.); andreastefano.basso@polimi.it (A.B.P.)

<sup>2</sup> Department of Organic Chemistry, Aachen-Maastricht Institute for Biobased Materials (AMIBM), Maastricht University, Urmonderbaan 22, 6167 KD Geleen, The Netherlands; r.orrù@maastrichtuniversity.nl

<sup>3</sup> Department of Materials Science, INSTM, Università degli Studi di Milano Bicocca, Via R. Cozzi 55, 20125 Milano, Italy; roberto.scotti@unimib.it

<sup>4</sup> Department of Engineering “Enzo Ferrari”, Università degli Studi di Modena e Reggio Emilia, Via Vivarelli 10/1, 41125 Modena, Italy; simone.pedrazzi@unimore.it (S.P.); marco.puglia@unimore.it (M.P.)

<sup>5</sup> Department of Civil, Chemical and Environmental Engineering—DICCA, Università di Genova (UniGe), Via All’Opera Pia 15, 16145 Genova, Italy; elisabetta.finocchio@unige.it

\* Correspondence: marianna.guagliano@polimi.it (M.G.); saverio.latorrata@polimi.it (S.L.)

**Abstract:** Adsorption is one of the simplest and most cost-effective techniques for water decontamination. In this field, biochar has recently emerged as a promising alternative to traditional adsorbents, exhibiting a high surface area and affinity to metal ions, as well as often being waste-derived. Similarly, reduced graphene oxide (rGO) shows an excellent adsorption capacity. Having self-assembling properties, it has already been employed to obtain self-standing heavy-metal-adsorbing membranes. In this research, a novel self-standing membrane of biochar and rGO is presented. It was obtained through an eco-friendly method, consisting of the simple mechanical mixing of the two components, followed by vacuum filtration and mild drying. Vine pruning biochar (VBC) was employed in different rGO/biochar mass ratios, ranging from 1/1 to 1/9. The best compromise between membrane integrity and biochar content was achieved with a 4/6 proportion. This sample was also replicated using chestnut-shell-derived biochar. The composite rGO–biochar membranes were characterized through XRD, FTIR-ATR, TG-DTG, SEM-EDX, BET, ZP, particle dimension, and EPR analyses. Then, they were tested for metal ion adsorption with 10 mM Cu<sup>2+</sup> and 100 mM Zn<sup>2+</sup> aqueous solutions. The adsorption capacity of copper and zinc was found to be in the range of 1.51–4.03 mmol<sub>Cu</sub> g<sup>−1</sup> and 18.16–21.99 mmol<sub>Zn</sub> g<sup>−1</sup>, respectively, at an acidic pH, room temperature, and contact time of 10 min. Interestingly, the composite rGO–biochar membranes exhibited a capture behavior between that of pure rGO and VBC.

**Keywords:** biochar; reduced graphene oxide; freestanding membrane; self-assembling; heavy metals; adsorption; water treatment



Academic Editors: Guangzhao Wang, Xiangkai Kong and Ning Wang

Received: 14 March 2025

Revised: 23 April 2025

Accepted: 27 April 2025

Published: 30 April 2025

**Citation:** Dotti, A.; Guagliano, M.; Ferretti di Castelferretto, V.; Scotti, R.; Pedrazzi, S.; Puglia, M.; Orrù, R.V.A.; Cristiani, C.; Finocchio, E.; Basso Peressut, A.; et al. Self-Standing Adsorbent Composites of Waste-Derived Biochar and Reduced Graphene Oxide for Water Decontamination. *Molecules* **2025**, *30*, 1997. <https://doi.org/10.3390/molecules30091997>

**Copyright:** © 2025 by the authors. Licensee MDPI, Basel, Switzerland. This article is an open access article distributed under the terms and conditions of the Creative Commons Attribution (CC BY) license (<https://creativecommons.org/licenses/by/4.0/>).

## 1. Introduction

The release of heavy metals is a highly hazardous outcome of many human activities, spanning from industrial production (e.g., mining and smelting) to agriculture (e.g., fertilization) [1]. Soil represents the ultimate sink for the environmental accumulation of heavy

metals, acting as the primary channel through which they spread to living organisms, the atmosphere, and water bodies [2]. Bioaccumulation in fruits and vegetables, drinking contaminated water, and direct ingestion or inhalation are the main pathways through which heavy metals enter the human body, posing a severe threat to human health [2–5]. Although some of these metal elements, such as Zn, Fe, Cu, and Cr, are necessary for the proper operation of certain biochemical functions, the accumulation of a few milligrams of these in the human body can become toxic [5]. An excessive ingestion of copper, for example, can lead to stomach, liver, and intestinal damage, as well as to skin cancer and angiosarcoma in the worst cases [2]. The accumulation of  $\text{Cu}^{2+}$  and  $\text{Zn}^{2+}$ , in particular, is mainly caused by their use in the livestock industry. In particular, in pig farming, these metals are added to the animal feed, for example in the form of inorganic salts, zinc chelate of hydroxy analogue of methionine, and copper chelate of hydroxy analogue of methionine, to boost the content of minerals in their diet to improve their growth, and strengthen their immune system [1,6–10]. Although these metal ions are essential for the well-being of the animals, only about 10%, mainly for the inorganic salts, is adsorbed and the remaining part is excreted via excrement. Since a small amount of  $\text{Cu}^{2+}$  and  $\text{Zn}^{2+}$  administered is actually absorbed by the pigs, most of it ends up in their excrement and, accordingly, in the environment [11–14]. If pig manure is used as fertilizer, metal ions can bioaccumulate in soil, and when they are consequently adsorbed by crops, they enter the food chain and have adverse health effects on natural organisms and humans, such as permanent organ damage, in particular to the kidneys, and disruptions to the immune system [11–14].

Moreover, the Intermediate Dynamic Model for Metal (IDMM) [15] predicted that zinc tends to accumulate more in the acidic sandy soils than other soil types after the use of treated manure, showing a greater tendency to drain and runoff into surface water [10].

In this scenario, it is essential to identify a proper method to remove  $\text{Cu}^{2+}$  and  $\text{Zn}^{2+}$ , preventing their spread into the environment [6,7].

Heavy metal removal can be carried out with conventional technologies, including chemical precipitation, ion exchange, adsorption, coagulation, and flocculation, as well as electrochemical processes, or with more recent strategies, such as biosorption or photocatalysis [16,17]. Among these, adsorption-based methods appear to be the most promising because of their low cost, high efficiency, simple operation, low consumption of solvents, high recovery efficiency, fast extraction time, and the possibility of regenerating sorbents [18–20]. An innovative and environmentally friendly adsorbent material is biochar (BC), the carbonaceous porous by-product of the residual biomass gasification process, characterized by an extraordinarily high porosity, large surface area, and high recalcitrance [21]. In addition, biochar shows a high affinity both with organic molecules [22–26] and heavy metals [18,27–31].

However, the practical application of biochar in wastewater treatment is currently limited [32] due to its low density and small particle size, which hinder its separation from water [33]. Being an effective adsorbent for contaminants, BC can act as an active carrier for pollutants. This results, through a co-transportation mechanism, in increased water and soil pollution [34]. Recovering the sorbent material still appears to be the most difficult step in the implementation of water treatment processes employing biochar [35]. In order to minimize environmental safety risks and to enable material reuse, biochar particles should be immobilized in macrostructures. Biochar-based membranes, in particular, appear as a promising strategy to limit the shedding and transport of fine BC particles, while preserving its excellent adsorption capability [36]. Mixed matrix membranes have been mainly developed by dispersing biochar particles as active fillers in a continuous phase. Typically, polymeric materials are used for the continuous phase, namely polyvinyl chloride (PVC) [37], polyvinylidene fluoride (PVDF) [38], polydopamine (PDA) [39], or

polysulfone (PSF) [40]. However, biochar/polymer composite membranes may be subject to the common drawbacks of polymeric membranes, such as their swelling in solvents and decomposition at high temperatures and critical pH conditions, which would exclude many application fields [1]. Moreover, excluding the one proposed by Ghaffar et al. [38] and Saad et al. [41], all the above-mentioned membranes require a support material, e.g., glass.

Reduced graphene oxide (rGO) has attracted great interest for water purification applications in the last decade [42–44]. It can be effectively employed to capture organic molecules and metal ions [45,46]. Moreover, showing self-assembling properties, rGO can assemble in self-standing membranes, without compromising its adsorption capacity [47–49]. Coupling biochar (BC) with rGO presents multiple advantages. Compared to BC alone, rGO is responsible for an improvement of the adsorption performances in rGO–BC composites [50–55]. Furthermore, the self-assembling ability of rGO can be exploited to obtain self-standing rGO–BC objects [56,57].

The aim of this work is to obtain a self-assembling rGO–biochar membrane through a simple and eco-friendly process. For this purpose, different ratios between biochar and rGO were evaluated to find the best compromise between the maximization of biochar content and the preservation of the self-assembling properties of the membrane. Pristine materials and membranes were characterized by means of X-ray diffraction (XRD), scanning electron microscopy and energy-dispersive X-ray analysis (SEM-EDX), Fourier-transform infrared spectroscopy in attenuated total reflectance (FT-IR ATR), and thermogravimetric analysis (TG-DTG).

Moreover, aqueous solutions with  $\text{Cu}^{2+}$  and  $\text{Zn}^{2+}$ , whose contents are similar to the real metal concentrations in piglets' manure found in a rearing system in Northern Italy [11], have been tested to assess the metal ion removal properties of the proposed membranes. The  $\text{Cu}^{2+}$  adsorption was also evaluated by electron paramagnetic resonance (EPR) measurements.

Our innovative approach develops self-standing membranes composed of biochar, a sustainable and cost-effective material, and rGO, a well-known material with self-assembling and adsorption capabilities. Even though a combination of biochar and rGO has already been explored in the literature [58], to the best of our knowledge, this is the first study carried out to develop rGO–biochar freestanding membranes just by mixing rGO and biochar for wastewater treatment applications.

## 2. Results and Discussion

### 2.1. Membrane Preparation

Mixed membranes containing different amounts of reduced graphene oxide and vine pruning biochar were produced. Starting from 50% *w/w*, the vine pruning biochar (VBC) content was progressively increased to 60, 70, 80, and 90% *w/w*; samples representing the two limit conditions, i.e., 100% rGO and 100% VBC, were also prepared. The 100% VBC suspension did not allow the formation of a membrane, confirming that biochar has no self-assembly capability. Conversely, all the rGO-based suspensions were able to form a quite uniform membrane layer, which could be peeled off from the PVDF supporting membrane. Remarkably, even 10% rGO was enough to obtain a membrane with self-assembling capabilities. Nevertheless, the membranes were cracked and damaged for a VBC content equal to or higher than 70% and thus were difficult to handle. Samples with VBC contents of 50% and 60%, in contrast, were resistant enough to endure manipulations without cracking. Considering that the target was to replace rGO with the highest biochar content, the membrane with a mass ratio of  $\text{rGO/VBC} = 40/60$  (rGO–VBC, Figure 1a) was considered to have the best result. Similarly, an intact and self-standing membrane was obtained by replacing 60% of rGO with chestnut-waste-derived biochar (rGO–CBC,

Figure 1b). This suggests that the self-assembling properties of the system are not affected by the biochar's characteristic, but are mainly dependent on the content of rGO, which is able to exert its assembly capability up to this mass ratio. Accordingly, rGO-VBC and rGO-CBC membranes were characterized and tested for metal adsorption.

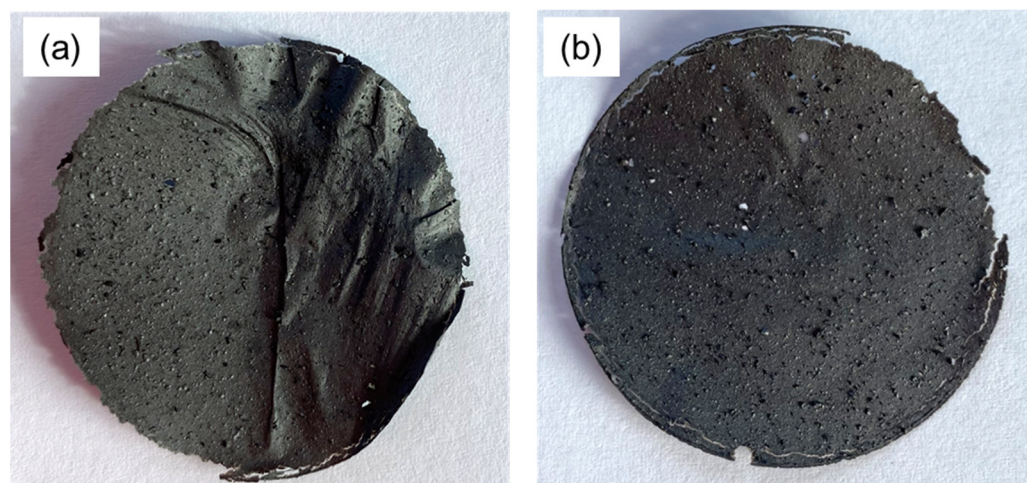


**Figure 1.** rGO-BC membranes with 60% biochar content: (a) vine pruning biochar (rGO-VBC) and (b) chestnut shell biochar (rGO-CBC).

## 2.2. Pristine Material and Membrane Characterization

In Table 1, the surface area (SA), particle dimensions, and zeta potential (ZP) of pristine VBC and CBC are reported.

**Table 1.** Surface area, particle dimensions, and zeta potential of vine pruning (VBC) and chestnut shell (CBC) biochar (\* pH of biochar in distilled water).

Sample	SA (m <sup>2</sup> g <sup>−1</sup> )	Particle Dimensions	Zeta Potential (mV)
		d <sub>10</sub> , d <sub>50</sub> , d <sub>90</sub> (μm)	
VBC	28	6, 31, 66	−39 (* pH 8)
CBC	327	2, 25, 64	−6 (* pH 11)

The two biochars exhibit different properties (Table 1). CBC shows a very high surface area, more than one order of magnitude greater than the one of VBC. This may indicate the presence of undecomposed biomass in the VBC sample, which possibly resulted in the clogging of pores. The values for the VBC's zeta potential support this picture. In fact, the ZP value has been related to the nature and the number of surface functional groups, meaning that a highly negative ZP corresponds to a large number of negatively charged groups, which are abundant in undecomposed biomass [59]. Moreover, the absolute value of ZP has been reported to increase when lowering the pyrolysis temperature [59]. Thus, the presence of undecomposed biomass in VBC is in accordance with its high ZP value (−39 mV). On this basis, it can be speculated that the VBC sample was obtained at a lower pyrolytic temperature than CBC.

In Figure 2, the X-ray diffraction patterns the pristine materials and of the 40/60 rGO-VBC and rGO-CBC membranes are reported.

In both XRD patterns of the pristine biochars, the broad reflections centered between 22 and 26 2θ° and at about 43 2θ° are consistent with the presence of graphite layers, as a result of the biomass decomposition [60]. Furthermore, the reflections at 23, 29.4, 35.9, and 47.5 2θ°, which are stronger and better defined in VBC than in CBC, are consistent



with the presence of a polycrystalline  $\text{CaCO}_3$  calcite-like phase containing impurities of Mg ions [61]. As a matter of fact, inorganic phases, such as calcite, are formed by the natural inorganic components, mainly Ca and Mg, of the biomass cells. Finally, the reflections at 22 and 26  $2\theta^\circ$  could be attributed to residual cellulose and hemicellulose that partially overlap the graphite layers [60,62].

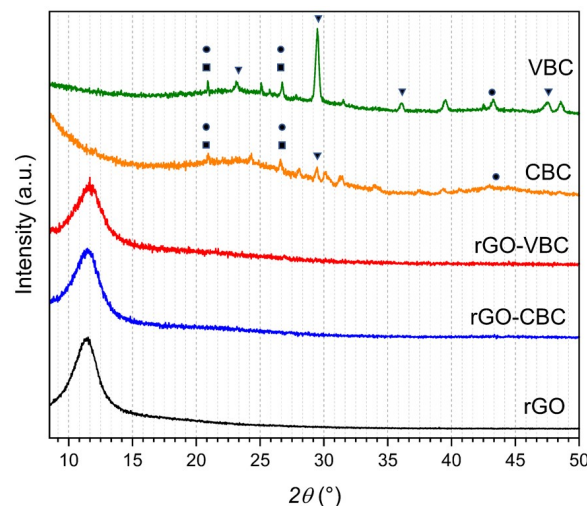


**Figure 2.** XRD patterns of pristine components and rGO–biochar mixed membranes (● graphite; ▼ calcite and dolomite; ■ hemicellulose and cellulose).

In the case of the rGO diffractogram, only the typical intense reflection at 11.3  $2\theta^\circ$ , corresponding to the (001) plane of rGO [56], is detected. This reflection is the only one detected in the XRD patterns of the mixed membranes (11.6 and 11.5  $2\theta^\circ$  for rGO–CBC and rGO–VBC, respectively), and no reflections related to the calcite or graphite phases are detected. This finding may be ascribed to the lower content of biochar (60%) in the mixed membranes, compared with pristine biochar, which make calcite and graphite detection improbable.

The thermograms obtained from the TGA of the nitrogen of the pristine biochars (VBC and CBC), the rGO, and the corresponding membranes (rGO–VBC and rGO–CBC) are compared in Figure 3. Biochar thermograms are characterized by a continuous weight loss of about 10–20% (Figure 3a). In contrast, the decomposition curve of the pristine rGO shows a high weight loss, about 70%, characterized by three steps.

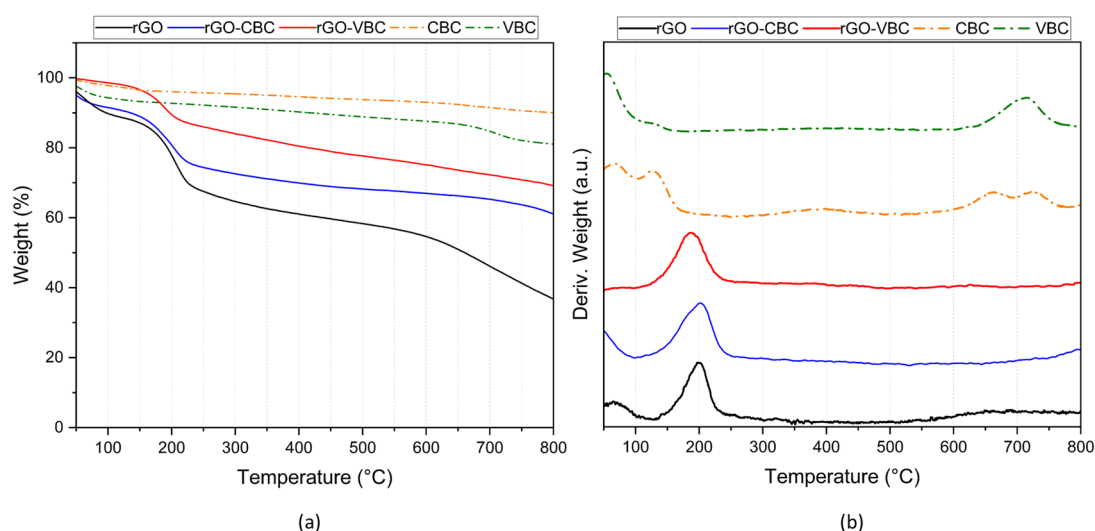


**Figure 3.** (a) TG and (b) DTG curves of pristine biochar and of rGO–biochar mixed membranes.

The thermal decomposition features of the mixed membranes are intermediate between those of rGO and biochars. The thermal decomposition behavior of the samples, especially in the case of the mixed membranes, can be better analyzed by DTG, as shown in Figure 3b, in which thermal phenomena are highlighted. The DTG results can be summarized as follows: (i) the thermal phenomenon, in the range of 30–100 °C, which is common across all the samples, is associated with the evolution of physiosorbed water molecules; (ii) the strong phenomenon between 150 and 250 °C may account for the decomposition of the residues of ascorbic acid and oxygenated moieties present in rGO [47,63]; (iii) the broad and barely visible phenomenon occurring above 600 °C can be ascribed to the degradation of the graphitic framework; (iv) finally, the phenomenon in the range of 650–750 °C may correspond to the thermal decomposition of traces of the calcite phase in biochars [64].

The pristine components and mixed membranes were also analyzed by FT-IR spectroscopy in ATR mode (Figure 4).

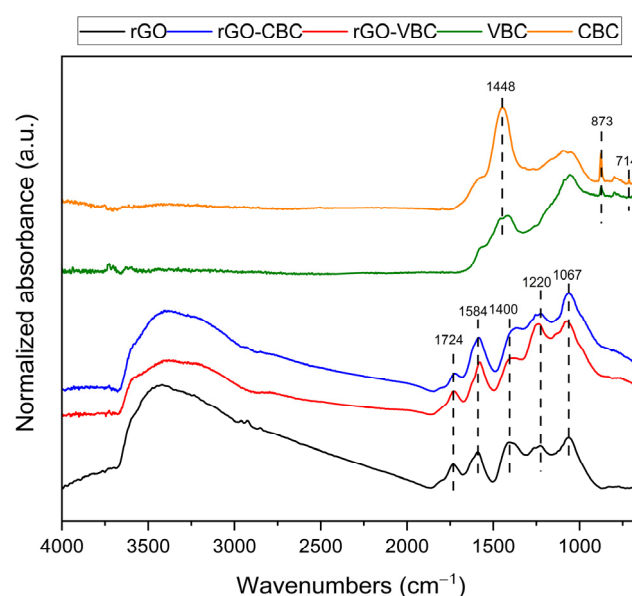


**Figure 4.** FT-IR ATR spectra of pristine components and rGO–biochar mixed membranes.

The pristine biochars exhibit very similar spectra, characterized by a main band centered around 1448  $\text{cm}^{-1}$ , accompanied by a sharp band at 873  $\text{cm}^{-1}$ , and weak components near 714  $\text{cm}^{-1}$ , which are characteristic of carbonate species [65]. The broad envelope of bands in the spectral region of 1200–1000  $\text{cm}^{-1}$  can be due to the overlapped CC and CO stretching modes, together with ring vibration and COH deformation, assigned to the residual cellulosic material. These findings also support the results of the XRD analysis [66].

In contrast, the spectrum of rGO is characterized by the presence of several bands, all of them consistent with those reported in the literature for graphene oxide [59]. The reduction treatment by L-AA leads indeed to a significant decrease in the intensity of these features, which are due to residual oxygen-containing groups. Specifically, the bands centered at 1067 and 1220  $\text{cm}^{-1}$  are associated with the C–O stretching vibrations of residual hydroxyl and alkoxy groups [67]. The contributions at about 1400, 1584, and 1724  $\text{cm}^{-1}$  might refer to, respectively, the C–H bending of alkyl chains and/or O–H deformation modes of carboxylic groups, C=C stretching in graphene oxide layers, and C=O stretching in carboxylic and carbonyl groups [47,68]. Finally, the broad and strong absorption band between roughly 3000 and 3500  $\text{cm}^{-1}$  may be attributed to O–H stretching modes [47,67,68].

The bands detected in the spectra of the composite membranes are consistent with those of rGO, while the biochar features are no longer clearly detected. It can be speculated

that the biochar features overlap those of rGO, with the latter being quite intense. This would explain the general increase in the region of  $1250\text{--}1000\text{ cm}^{-1}$ . The absence of carbonate species is likely due either to their dissolution in the slightly acidic, reduced GO suspension during the preparation procedure or to a possible inhomogeneous distribution in the analyzed membrane portion.

SEM images from backscattered electrons, secondary electrons, and SEM-EDX analyses of the rGO, rGO-VBC, and rGO-CBC membranes are reported in Figure 5a–c.

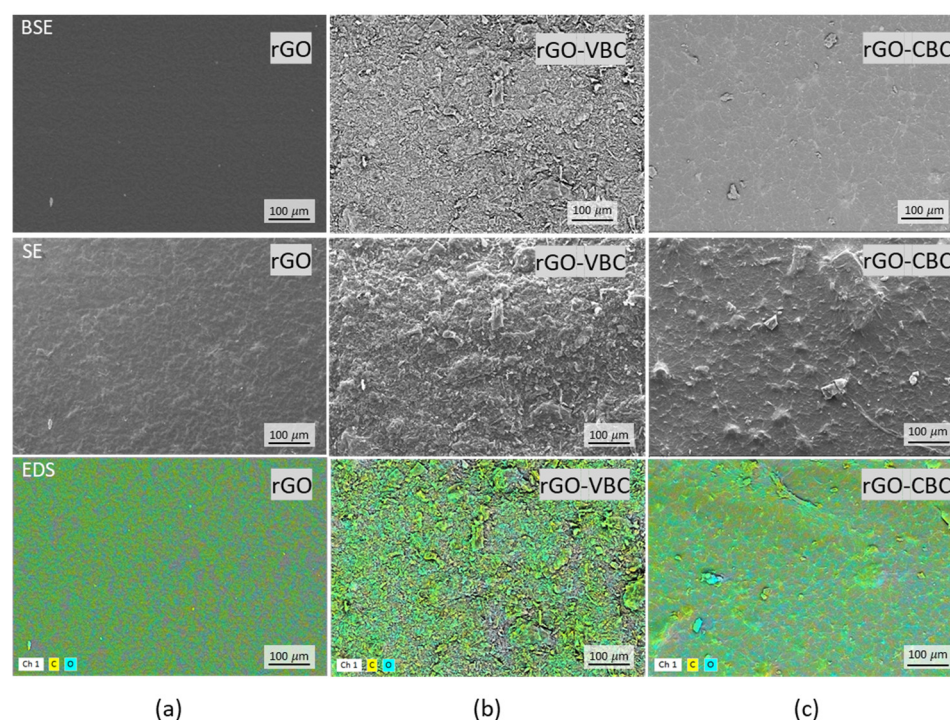


**Figure 5.** SEM-EDX images at  $500\times$  magnification of (a) rGO, (b) rGO-VBC, and (c) rGO-CBC. Backscattered electrons (**top**), secondary electrons (**middle**), and EDX maps indicating carbon in yellow and oxygen in light blue (**bottom**).

The surface of the rGO membrane (Figure 5a, top and middle) appears as a continuous, flat, and homogeneous layer, without distinguishable cracks or aggregates. Carbon and oxygen are uniformly distributed on the surface (Figure 5a, bottom). Conversely, the surface of both the mixed rGO-VBC and rGO-CBC membranes (Figure 5b,c) is characterized by an irregular morphology, in which the presence of aggregates, although apparently incorporated in a matrix, is manifest (Figure 5b,c, top and middle). Aggregates are much more appreciable in the case of the rGO-VBC membrane (Figure 5b), whose surface morphology and elemental distribution in the EDX map (Figure 5b, bottom) appear to be more heterogeneous. The presence of a continuous matrix incorporating the aggregates is consistent with the self-assembly effect exerted by rGO, which apparently is not perturbed by the presence of biochar. In this respect, it has to be noted that the pristine biochars, both CBC and VBC, are not able to form freestanding films.

### 2.3. $\text{Cu}^{2+}$ and $\text{Zn}^{2+}$ Adsorption Tests

rGO-VBC membranes with a 60% content of biochar, being selected as the best compromise between maximizing VBC and sample resistance to manipulation, were employed in  $\text{Cu}^{2+}$  and  $\text{Zn}^{2+}$  adsorption tests in mono-ionic aqueous solutions. Pristine rGO and VBC were also tested for comparison. Each sample was put in contact with a 50 mL solu-

tion containing either 62.5 mmol g<sup>-1</sup> of Cu<sup>2+</sup> or 625.0 mmol g<sup>-1</sup> of Zn<sup>2+</sup>. The solutions' compositions were selected to simulate real ion concentrations in weaned pigs sludge [11].

The specific captured amount of metal ions  $Q_m$  (mmol g<sup>-1</sup>) for each sample was obtained via Equation (2). Moreover, the theoretical adsorption capacity  $Q_{m,th}$  for the rGO–VBC mixed membrane was calculated according to Equation (1), considering the experimental  $Q_m$  values of rGO and VBC.

$$Q_{m,th}(rGO - VBC) = 0.40 \cdot Q_m(rGO) + 0.60 \cdot Q_m(VBC) \quad (1)$$

Experimental and theoretical capacities are summarized in Table 2.

**Table 2.** Cu<sup>2+</sup> and Zn<sup>2+</sup> capture ( $Q_m$ ) by VBC as function of the initial ions' concentrations (\*  $Q_{m,th}$  theoretical adsorption capacity via Equation (2)).

Sorbent	Cu <sup>2+</sup>			Zn <sup>2+</sup>		
	Initial Cu <sup>2+</sup> (mmol g <sup>-1</sup> )	$Q_m$ (mmol g <sup>-1</sup> )	$Q_{m,th}$ * (mmol g <sup>-1</sup> )	Initial Zn <sup>2+</sup> (mmol g <sup>-1</sup> )	$Q_m$ (mmol g <sup>-1</sup> )	$Q_{m,th}$ * (mmol g <sup>-1</sup> )
rGO	62.5	4.03	-	625.0	18.16	-
VBC		1.51	-		21.99	-
rGO–VBC		2.19	2.52		19.12	20.46

All the sorbents show a low sorption efficiency, in the range of 3–6%, and rGO–VBC exhibits an intermediate level of adsorption between the levels of the pristine components. The low capture percentages are apparently far from those reported in the literature, with the initial concentrations selected for these experiments (Cu<sup>2+</sup> 10 mM and Zn<sup>2+</sup> 100 mM) being considerably higher than those applied in previous studies (in the range of 0.1–3 mM) [69–71]. Also, the particular testing setup employed in this research makes comparisons of efficiency with other studies difficult and not very representative.

During the experiments, the pH values of the solutions were measured before and after the adsorption tests (Table 3).

**Table 3.** pH values of Cu<sup>2+</sup> and Zn<sup>2+</sup> solutions before and after the filtration tests.

Ion	pH Before Tests	pH After Test		
		rGO	VBC	rGO–VBC
Cu <sup>2+</sup>	4.6	2.9	4.8	2.9
Zn <sup>2+</sup>	4.9	2.9	5.4	3.8

It is evident that the solution pH during the contacting experiment is driven by the solid sorbent; indeed, before the tests, it is weakly acidic, in the range of 4.6–4.9. Once the solutions are put in contact with the sorbent, the sorbent nature modifies the pH in view of the acidity/basicity of the surface. It can be hypothesized that, in the case of rGO, the pH strongly decreased in view of the presence of the residual amount of L-ascorbic acid used for the reduction, which is released during the tests. In contrast, the slight pH increase observed for VBC can be explained by the presence of the residual amount of calcite. Indeed, nitrates present in the contacting solution are able to displace calcite carbonates, so that calcium ions' dissolution induces the slight pH increase. In the case of the mixed membrane, the acidification due to the rGO component is predominant, in particular for Cu<sup>2+</sup>. This last observation could be related either to slight differences in the



membrane composition, as the two tests have been performed on two different membranes, or to the higher basicity of Zn ions.

The low capture capability of the mixed membrane does not seem to be caused by the poor stability of the membrane. Indeed, as reported in the literature, rGO membranes tend to remain stable over time and in different pH conditions [72–75]. Biochar is considered to be a stable material as well. However, its stability may vary with other properties, such as its surface area, pH, and porosity. A method to assess biochar's stability involves the evaluation of its aromatic characteristics, as shown in both VBC and CBC by XRD analysis, which usually become more pronounced at higher pyrolysis temperatures [76,77]. Furthermore, research concerning the combination of rGO and biochar has demonstrated the formation of stable materials [41,78].

Conversely, the low capture capability of the mixed membrane can be justified considering the membrane's composition, i.e., 60% *w/w* of VBC and 40% *w/w* of rGO. As a matter of fact, the theoretical adsorption capacity of the mixed membrane, being the combination of those of the single components, is negatively affected by the limited rGO content, i.e., the most efficient sorbent (Table 2).

However, the actual adsorptions  $Q_m$  of rGO–VBC, 2.19 for  $\text{Cu}^{2+}$  and 19.12  $\text{mmol g}^{-1}$  for  $\text{Zn}^{2+}$ , are consistent with  $Q_{m,th}$ , i.e., 2.52  $\text{mmol g}^{-1}$  and 20.46  $\text{mmol g}^{-1}$  for  $\text{Cu}^{2+}$  and  $\text{Zn}^{2+}$ , respectively. This may suggest that neither synergistic nor antagonistic effects are present, and the adsorption capacity of rGO–VBC is just the weighted sum of the capacities of the single components. Therefore, despite the thorough mixing observed by SEM-EDX (Figure 5b), the components are just mixed and, apparently, they do not interact with each other.

The capture yield of the different sorbents has been calculated and is plotted in Figure 6.

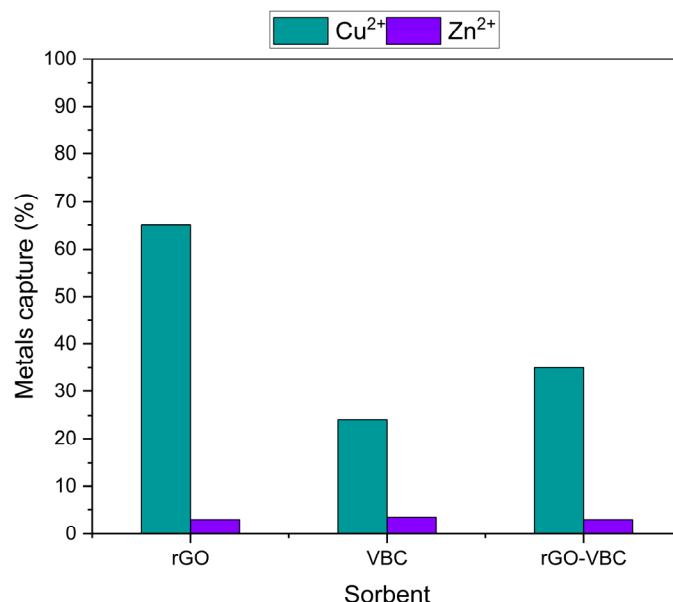


**Figure 6.** Metal capture efficiency of the different sorbents.

Comparing the Zn and Cu yield results, it is evident that Cu capture is much more efficient than Zn capture for all the sorbents. The best Cu capture is obtained by the use of rGO (65%), and it is only partially preserved in the mixed membrane. Instead, a very low and constant Zn capture (about 3%) was found. It can be argued that all the sorbents possess a higher affinity for Cu than for Zn, but it has to be noted that the initial Zn content is two orders of magnitude higher than the Cu content (6.25 and 625  $\text{mmol g}^{-1}$  for Cu and Zn, respectively). Furthermore, the constant Zn adsorption suggests the presence of a site

saturation effect, but all these considerations need to be confirmed in further studies with solutions at different initial concentrations. However, the presence of a selectivity effect is of paramount importance when the two ions are co-present in solution, as in the case of real sludges.

Moreover, although the study of adsorption isotherms is not the primary focus of this work, we expect that the materials could demonstrate behavior consistent with Langmuir and Freundlich adsorption isotherms, as reported in the literature [52,70,79,80].

The membranes after the adsorption experiments were characterized by means of SEM-EDX spectroscopy (Figure 7a–c). The images confirm the presence of  $\text{Cu}^{2+}$  (Figure 7a–c, top, blue spots) and  $\text{Zn}^{2+}$  (Figure 7a–c, bottom, pink spots) on the sorbents' surface. Cu is uniformly distributed onto the rGO membrane (Figure 7a, top), while is apparently localized in specific areas in the case of the pristine VBC (Figure 7c, top). Similarly, for  $\text{Zn}^{2+}$  ions, the metal is quite homogeneously distributed on the rGO membrane, but it is clearly adsorbed in specific areas in the VBC (Figure 7c, bottom). The mixed rGO–VBC membranes again feature an intermediate situation (Figure 7b), in which the homogeneous distribution of the ions coexists with local accumulation and clustering. This is particularly evident in the case of  $\text{Zn}^{2+}$  (Figure 7b, bottom).

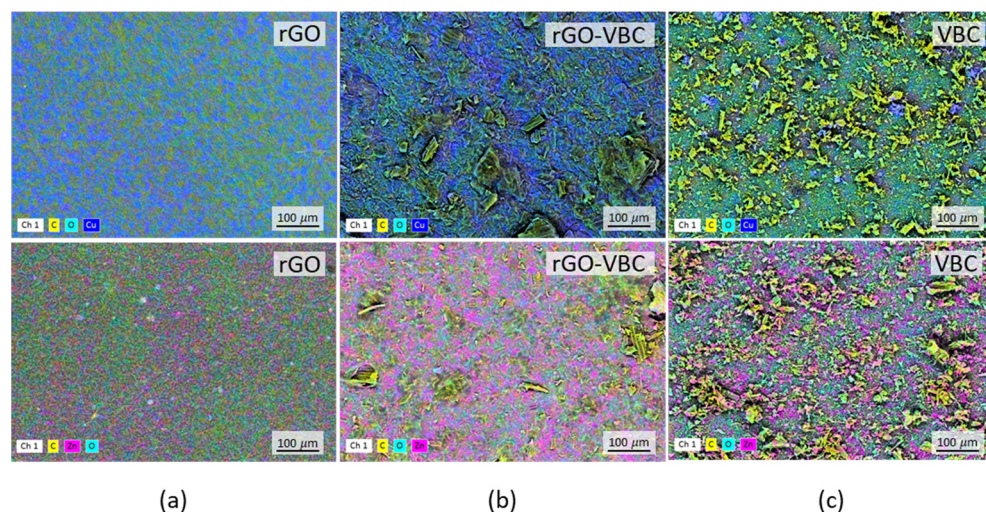


**Figure 7.** SEM-EDX elemental maps at 500 $\times$  magnification of (a) rGO, (b) rGO–VBC, and (c) VBC after adsorption of  $\text{Cu}^{2+}$  (top, blue spots) and  $\text{Zn}^{2+}$  (bottom, pink spots).

Analyzing the EDX maps, it is hard to find a correlation between functional groups, namely the oxygenated ones, which are presumably those capable of interacting with the ions, and adsorption sites. Indeed, as shown in the maps, the light blue spots, corresponding to oxygen, are homogeneously spread on the surface of all the solids, and no correlation between the surface area elemental composition and the formation of adsorbed ions' clusters is visible.

Considering the difficulty of obtaining information on the adsorption sites, the membranes after copper adsorption were also evaluated by electron paramagnetic resonance (EPR) spectroscopy. The EPR spectra of VBC in powder form as well as of rGO–VBC and rGO membranes after the adsorption of a 10 mM solution of  $\text{Cu}^{2+}$  are reported in Figure 8, comparing them with the spectra of the bare biochar powder and the as-prepared rGO–VBC membrane as a blank. The spectra of all samples containing biochar show typical isotropic signals at  $g = 2.023$  due to the carbon-centered permanent free radicals (PFR) of biochar [81,82], either before or after Cu adsorption. After the adsorption of copper, the EPR spectra of all the membranes show the presence of  $\text{Cu}^{2+}$  species, with an intensity which confirms the trend of copper adsorption obtained by ICP-OES analysis. In particular,

the copper EPR signal in VBC powder has the lowest intensity compared to those of the rGO–VBC and rGO membranes. The adsorbed Cu signal exhibits values of  $g_{||} = 2.27$ ,  $g_{\perp} = 2.10$ , and resolved parallel hyperfine structures  $A_{||} = 170$  G, which can be assigned to  $\text{Cu}^{2+}$  centers with tetragonally distorted octahedral symmetry [83]. On the other hand, the EPR copper spectra of both rGO–VBC and rGO are characterized by the overlapping of  $\text{Cu}^{2+}$  center signals similar to those in VBC powder and by a broad and unstructured line centered at  $g \approx 2.15$ , which is typical of dipolar coupled  $\text{Cu}^{2+}$  species with a disordered coordination environment and is likely related to the highest amount of copper adsorbed by the two membranes [84].

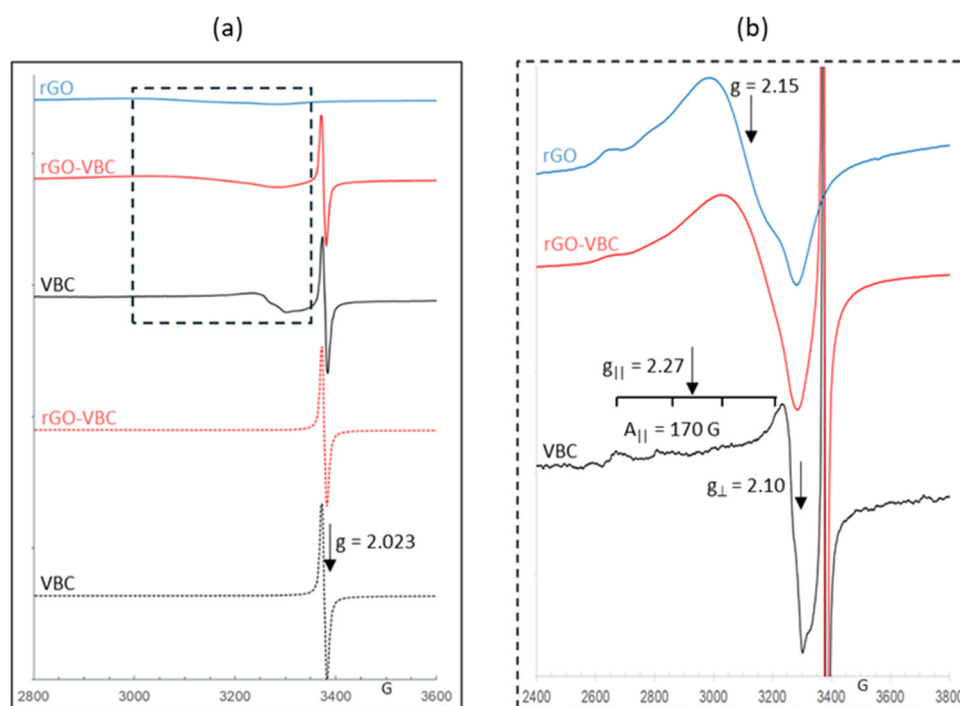


**Figure 8.** (a) EPR spectra of sorbents before (dotted lines) and after (solid lines)  $\text{Cu}^{2+}$  adsorption tests; (b) magnification, corresponding to the dashed line box, of  $\text{Cu}^{2+}$  spectra.

### 3. Materials and Methods

#### 3.1. Materials

A commercial biochar (VBC), produced via a proprietary process from vine pruning biomass, was supplied by Romagna Carbone (Bagnacavallo, RA, Italy). Chestnut biochar (CBC) was prepared at the BEELab of Modena and Reggio Emilia University by a gasification process (with maximum temperature of 800–1000 °C) using chestnut shells and pericarps (provided by Az. Agr. Agriappennino di Sepe Marco, Cecciola, RE, Italy) as feed biomass. In particular, it was pelletized to be used as fuel in a fixed-bed downdraft gasifier prototype. It has an Imbert-throated hearth reactor designed to operate with a biomass flow of a few  $\text{kg h}^{-1}$ , making it ideal for testing when only a limited amount of fuel is available [85]. Graphene oxide in the form of a  $4 \text{ mg mL}^{-1}$  aqueous dispersion (particle size  $< 10 \text{ }\mu\text{m}$ ) was acquired from Graphenea (San Sebastian, Spain). L-ascorbic acid (L-AA),  $\text{Cu}(\text{NO}_3)_2 \cdot 3\text{H}_2\text{O}$ , and  $\text{Zn}(\text{NO}_3)_2 \cdot 6\text{H}_2\text{O}$  were supplied by Sigma-Aldrich (Milan, Italy).

#### 3.2. Membranes Preparation

Membranes were prepared according to a simple previously developed protocol [47,86], which was adapted for the addition of biochar (Figure 9). In particular, the GO commercial dispersion, after dilution to  $0.4 \text{ mg mL}^{-1}$  and ultrasonication (Labsonic LBS1-6, Falc

Instruments, Faenza, Italy), was reduced with L-AA (L-AA:GO = 10:1 by weight). The suspension was stirred for 24 h at room temperature. Biochar, previously ground in a mortar until obtaining a uniform and fine powder, was added to the above suspension 30 min before the end of the stirring time. The mixture was then poured in a Gooch crucible and vacuum-filtered onto a polyvinylidene fluoride (PVDF) membrane with a 47 mm diameter and 0.45  $\mu\text{m}$  pore size (Merck Millipore, Burlington, MA, USA). The resulting membranes were dried in an oven for 2 h at 60  $^{\circ}\text{C}$ .

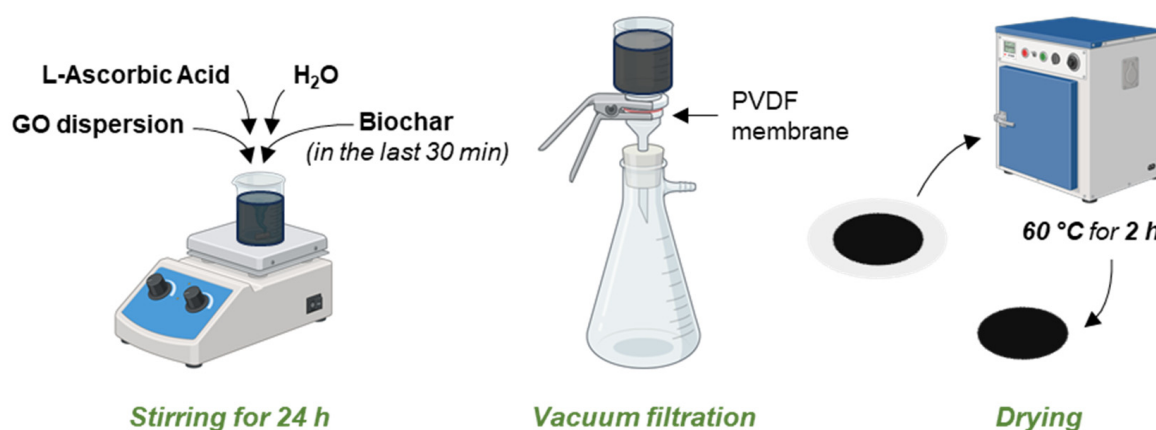


**Figure 9.** Membrane preparation procedure.

Setting a total membrane weight of 8 mg, different rGO/BC ratios were considered; namely, biochar was introduced to replace 50, 60, 70, 80, and 90% *w/w* rGO. Pure biochar and pure rGO samples were also prepared to be used as reference. Specifically, for the pure rGO membrane, the above-mentioned conventional procedure was applied, without the addition of BC. Conversely, for the pure biochar sample, 8 mg of BC was dispersed in H<sub>2</sub>O, then it was vacuum-filtered and dried as previously described.

### 3.3. Pristine Materials and Membranes Characterization

Surface area (SA) was measured by performing Brunauer–Emmett–Teller (BET) analysis (in N<sub>2</sub> atmosphere and bath temperature of 77.35 K) with the ASAP 2420 apparatus by Micromeritics (Norcross, GA, USA) on samples previously outgassed at 120  $^{\circ}\text{C}$  to a residual pressure of  $<10^{-4}$  Pa.

X-ray diffraction (XRD) patterns of the pristine powders were collected at room temperature in the range of 8–50 $^{\circ}$  2 $\theta$  through a D2-Phaser diffractometer (Bruker Italy, Milan, Italy), equipped with Cu radiation ( $\lambda = 1.54$  Å) using Bragg Brentano geometry.

Particles' dimensions were determined by laser granulometry (CILAS 1180 instrument, Orleans, France) according to Klank et al. [87].

Zeta potential (ZP) was determined using 5 mg L<sup>−1</sup> of biochar dispersed in water, at the pH of the solid in water, using a Zetasizer Nano ZS (Malvern Instruments Limited, Malvern, UK). Dynamic light scattering (DLS) at 90 $^{\circ}$ , with non-invasive backscatter (NIBS) optics, was used for measurements.

Macro-Fourier-transform infrared spectroscopy in attenuated total reflectance (ATR FT-IR) spectra were recorded using an FTIR Nicolet Nexus spectrometer, which was equipped with a single reflection silicon crystal, a mercury cadmium telluride (MCT) detector cooled with liquid nitrogen, and a ThermoElectron Continuum IR microscope, all supplied by Thermo Fisher Scientific Inc. (Rodano, Italy). Spectra were collected in the 650–4000 cm<sup>−1</sup> range with 128 scans and a spectral resolution of 4 cm<sup>−1</sup>.



Thermogravimetric analysis (TG-DTG) from room temperature up to 850 °C was performed using a TGAQ500 (TA Instruments, Eschbor, Germany) with a heating rate of 10 °C min<sup>−1</sup> in nitrogen atmosphere.

Scanning electron microscopy and energy-dispersive X-ray spectroscopy (SEM-EDX), before and after Cu<sup>2+</sup> and Zn<sup>2+</sup> capture tests, were performed using a Zeiss EVO 50 EP (Zeiss, Jena, Germany) equipped with an INCA energy 2000 spectrometer (Oxford Instruments, Abingdon-on-Thames, UK), operated at an electron high tension (EHT) voltage of 20 kV, with a current probe of 100 pA, and in high vacuum mode (10<sup>−4</sup> Pa).

Electron paramagnetic resonance (EPR) measurements were performed before and after Cu<sup>2+</sup> adsorption at 123 K using an EMX spectrometer (Bruker Italy, Milan, Italy) operating at the X-band frequency and equipped with an Oxford Instruments cryostat (Abingdon-on-Thames, UK). Spectra were recorded at a power of 2 mW, modulation amplitude 2 or 10 G, and at 130 K.

### 3.4. Adsorption Tests

For metal ions' adsorption tests, mono-ionic aqueous solutions of Cu<sup>2+</sup> 10 mM (635 mg L<sup>−1</sup>) and Zn<sup>2+</sup> 100 mM (6530 mg L<sup>−1</sup>), which are close to the real concentration values in piglets' manure [11], were prepared. Exploiting the same filtration setup reported in Figure 9, the adsorption experiments were carried out by putting each membrane in contact with 50 mL of mono-ionic solution for 10 min, which was poured into the Gooch crucible. Then, the solution was vacuum-filtered through the membrane. The pH values of the solutions, both as-prepared and after the contacting process, were measured (FiveEasy pH-meter equipped with an LE438 electrode, Mettler Toledo, Columbus, OH, USA), but no pH correction was applied.

Metal ions' concentration in solution was determined before ( $C_i$ ) and after ( $C_f$ ) the adsorption tests by means of inductively coupled plasma optical emission spectroscopy (ICP-OES) using an OPTIMA 7000 DV spectrometer (PerkinElmer, Waltham, MA, USA). Reported values are the average of three measurements, with an estimated error of 2.5%. The specific captured amount of metal ions  $Q_m$  (mmol g<sup>−1</sup>) was obtained according to Equation (2), where  $C_i$  (mg L<sup>−1</sup>) and  $C_f$  (mg L<sup>−1</sup>) are the initial and final ion concentrations, respectively,  $V$  is the volume of the contacted solution (50 mL),  $AW$  is the atomic weight of copper or zinc, and  $w_{\text{membrane}}$  is the membrane weight (8 mg).

$$Q_m \left( \text{mmol g}^{-1} \right) = \frac{(C_i - C_f) \cdot V}{AW \cdot w_{\text{membrane}}} \quad (2)$$

## 4. Conclusions

The membrane preparation procedure here proposed represents an innovative, simple, and low-environmental-impact strategy to immobilize biochar for water treatment applications. Indeed, in this study, the self-assembling properties of reduced graphene oxide were exploited to immobilize waste-derived biochar in a self-standing membrane. Different compositions were explored, considering a biochar mass percentage from 50 up to 90%. In all cases, self-standing membranes were successfully obtained, but the sample composed of 60% BC and 40% rGO showed the best compromise between membrane resistance and maximizing the biochar content, and this result was effectively obtained by employing both vine pruning and chestnut shell waste-derived biochars.

The mixed rGO–VBC membrane, when tested for water decontamination from Cu<sup>2+</sup> and Zn<sup>2+</sup> ions, showed intermediate adsorption properties (2.19 mmol g<sup>−1</sup> for Cu<sup>2+</sup> and 19.12 mmol g<sup>−1</sup> for Zn<sup>2+</sup>) between those of the two pristine components, which somewhat correspond to the theoretical one, calculated considering the mixed membrane composition.

Neither synergistic nor antagonistic effects on the capture capability are present in the mixed membrane, and the adsorption capacity of rGO–VBC is just the weighted sum of the capacities of the single components. Therefore, despite the thorough mixing observed by SEM-EDX, the components seem to be just mixed, with no apparent interactions between them.

A higher affinity for Cu than for Zn was found. The presence of a selectivity effect is crucial when the two ions are co-present in solutions, as occurs in real sludges. Thus, despite being preliminary, in the authors' opinion, this work represents a step forward for the technological valorization of waste-biomass-derived materials.

**Author Contributions:** Conceptualization, A.D., M.G., C.C. and S.L.; data curation, A.D. and M.G.; formal analysis, A.D., E.F., A.B.P. and S.L.; investigation, A.D., V.F.d.C., R.S., E.F. and A.B.P.; methodology, A.D., V.F.d.C., R.S. and A.B.P.; resources, R.S., S.P., M.P., C.C. and S.L.; supervision, R.V.A.O., C.C., E.F. and S.L.; validation, A.D. and M.G.; visualization, A.D., M.G., A.B.P. and S.L.; writing—original draft preparation, A.D., V.F.d.C., R.S. and C.C.; writing—review and editing, M.G., S.P., M.P., R.V.A.O., E.F., A.B.P. and S.L. All authors have read and agreed to the published version of the manuscript.

**Funding:** This research received no external funding.

**Institutional Review Board Statement:** Not applicable.

**Informed Consent Statement:** Not applicable.

**Data Availability Statement:** The data presented in this study are available on request from the corresponding authors.

**Conflicts of Interest:** The authors declare no conflicts of interest.

## Abbreviations

The following abbreviations are used in this manuscript:

BC	Biochar
CBC	Chestnut biochar
GO	Graphene oxide
L-AA	L-Ascorbic acid
rGO	Reduced graphene oxide
rGO–BC	Membrane composed of 40% rGO and 60% BC
rGO–CBC	Membrane composed of 40% rGO and 60% CBC
rGO–VBC	Membrane composed of 40% rGO and 60% VBC
SA	Surface area
VBC	Vine pruning biochar
ZP	Zeta potential

## References

1. Tchounwou, P.B.; Yedjou, C.G.; Patlolla, A.K.; Sutton, D.J. Heavy Metal Toxicity and the Environment. In *Molecular, Clinical and Environmental Toxicology. Experientia Supplementum*; Luch, A., Ed.; Springer: Basel, Switzerland, 2012; Volume 101. [\[CrossRef\]](#)
2. Ahmad, W.; Alharthy, R.D.; Zubair, M.; Ahmed, M.; Hameed, A.; Rafique, S. Toxic and Heavy Metals Contamination Assessment in Soil and Water to Evaluate Human Health Risk. *Sci. Rep.* **2021**, *11*, 17006. [\[CrossRef\]](#) [\[PubMed\]](#)
3. A Shakoob, M.B.; Ali, S.; Rizwan, M.; Abbas, F.; Bibi, I.; Riaz, M.; Khalil, U.; Niazi, N.K.; Rinklebe, J. A Review of Biochar-Based Sorbents for Separation of Heavy Metals from Water. *Int. J. Phytoremediat.* **2020**, *22*, 111–126. [\[CrossRef\]](#) [\[PubMed\]](#)
4. Gholizadeh, M.; Hu, X. Removal of Heavy Metals from Soil with Biochar Composite: A Critical Review of the Mechanism. *J. Environ. Chem. Eng.* **2021**, *9*, 105830. [\[CrossRef\]](#)
5. Gupta, S.; Sireesha, S.; Sreedhar, I.; Patel, C.M.; Anitha, K.L. Latest Trends in Heavy Metal Removal from Wastewater by Biochar Based Sorbents. *J. Water Process Eng.* **2020**, *38*, 101561. [\[CrossRef\]](#)
6. Provolto, G.; Manuli, G.; Finzi, A.; Lucchini, G.; Riva, E.; Sacchi, G. Effect of Pig and Cattle Slurry Application on Heavy Metal Composition of Maize Grown on Different Soils. *Sustainability* **2018**, *10*, 2684. [\[CrossRef\]](#)

7. Feng, Z.; Zhu, H.; Deng, Q.; He, Y.; Li, J.; Yin, J.; Gao, F.; Huang, R.; Li, T. Environmental Pollution Induced by Heavy Metal(Loid)s from Pig Farming. *Environ. Earth Sci.* **2018**, *77*, 103. [\[CrossRef\]](#)
8. European Commission. Commission Implementing Regulation (EU) 2021/968 of 16 June 2021 Concerning the Renewal of Zinc Chelate of Hydroxy Analogue of Methionine as a Feed Additive for All Animal species and repealing Regulation (EU) No 335/2010 (Text with EEA relevance)Text with EEA Relevance. *Off. J. Eur. Union* **2021**, *214*, 45–47.
9. European Commission. Commission Implementing Regulation (EU) 2023/1334 of 29 June 2023 Concerning the Renewal of the Authorisation of Copper Chelate of Hydroxy Analogue of Methionine as a Feed Additive for All Animal Species and Repealing Regulation (EU) No 349/2010. *Off. J. Eur. Union* **2023**, *166*, 111–115.
10. European Commission. *Commission Implementing Decision of 26.6.2017 Concerning, in the Framework of Article 35 of Directive 2001/82/EC of the European Parliament and of the Council, the Marketing Authorisations for Veterinary Medicinal Products Containing “Zinc Oxide” to Be Administered Orally to Food Producing Species (Text with EEA Relevance) ANNEX II*; European Commission: Brussels, Belgium, 2017.
11. Hejna, M.; Moscatelli, A.; Onelli, E.; Baldi, A.; Pilu, S.; Rossi, L. Evaluation of Concentration of Heavy Metals in Animal Rearing System. *Ital. J. Anim. Sci.* **2019**, *18*, 1372–1384. [\[CrossRef\]](#)
12. Gourlez, E.; Beline, F.; Dourmad, J.-Y.; Monteiro, A.R.; Guiziou, F.; Le Bihan, A.; De Quelen, F. The Fate of Cu and Zn along the Feed-Animal-Excreta-Effluent Continuum in Swine Systems According to Feed and Effluent Treatment Strategies. *J. Environ. Manag.* **2024**, *354*, 120299. [\[CrossRef\]](#)
13. Vardhan, K.H.; Kumar, P.S.; Panda, R.C. A Review on Heavy Metal Pollution, Toxicity and Remedial Measures: Current Trends and Future Perspectives. *J. Mol. Liq.* **2019**, *290*, 111197. [\[CrossRef\]](#)
14. Rai, P.K.; Lee, S.S.; Zhang, M.; Tsang, Y.F.; Kim, K.-H. Heavy Metals in Food Crops: Health Risks, Fate, Mechanisms, and Management. *Environ. Int.* **2019**, *125*, 365–385. [\[CrossRef\]](#) [\[PubMed\]](#)
15. Monteiro, S.C.; Lofts, S.; A Boxall, A.B. *Pre-Assessment of Environmental Impact of Zinc and Copper Used in Animal Nutrition*; EFSA Supporting Publication: Parma, Italy, 2010; Volume 7, p. 74E. [\[CrossRef\]](#)
16. Shrestha, R.; Ban, S.; Devkota, S.; Sharma, S.; Joshi, R.; Tiwari, A.P.; Kim, H.Y.; Joshi, M.K. Technological Trends in Heavy Metals Removal from Industrial Wastewater: A Review. *J. Environ. Chem. Eng.* **2021**, *9*, 105688. [\[CrossRef\]](#)
17. Zamora-Ledezma, C.; Negrete-Bolagay, D.; Figueroa, F.; Zamora-Ledezma, E.; Ni, M.; Alexis, F.; Guerrero, V.H. Heavy Metal Water Pollution: A Fresh Look about Hazards, Novel and Conventional Remediation Methods. *Environ. Technol. Innov.* **2021**, *22*, 101504. [\[CrossRef\]](#)
18. Biswal, B.K.; Balasubramanian, R. Use of Biochar as a Low-Cost Adsorbent for Removal of Heavy Metals from Water and Wastewater: A Review. *J. Environ. Chem. Eng.* **2023**, *11*, 110986. [\[CrossRef\]](#)
19. Riva, L.; Dotti, A.; Iucci, G.; Venditti, I.; Meneghini, C.; Corsi, I.; Khalakhan, I.; Nicastro, G.; Punta, C.; Battocchio, C. Silver Nanoparticles Supported onto TEMPO-Oxidized Cellulose Nanofibers for Promoting Cd<sup>2+</sup> Cation Adsorption. *ACS Appl. Nano Mater. J.* **2024**, *7*, 2401–2413. [\[CrossRef\]](#)
20. Thakur, A.; Kumar, A.; Singh, A. Adsorptive Removal of Heavy Metals, Dyes, and Pharmaceuticals: Carbon-Based Nanomaterials in Focus. *Carbon* **2024**, *217*, 118621. [\[CrossRef\]](#)
21. Gwenzi, W.; Chaukura, N.; Noubactep, C.; Mukome, F.N.D. Biochar-Based Water Treatment Systems as a Potential Low-Cost and Sustainable Technology for Clean Water Provision. *J. Environ. Manag.* **2017**, *197*, 732–749. [\[CrossRef\]](#)
22. Huang, Q.; Song, S.; Chen, Z.; Hu, B.; Chen, J.; Wang, X. Biochar-Based Materials and Their Applications in Removal of Organic Contaminants from Wastewater: State-of-the-Art Review. *Biochar* **2019**, *1*, 45–73. [\[CrossRef\]](#)
23. Celso Monteiro Zanona, V.R.; Rodrigues Barquilha, C.E.; Borba Braga, M.C. Removal of Recalcitrant Organic Matter of Landfill Leachate by Adsorption onto Biochar from Sewage Sludge: A Quali-Quantitative Analysis. *J. Environ. Manag.* **2023**, *344*, 118387. [\[CrossRef\]](#)
24. Behera, A.K.; Shadangi, K.P.; Sarangi, P.K. Efficient Removal of Rhodamine B Dye Using Biochar as an Adsorbent: Study the Performance, Kinetics, Thermodynamics, Adsorption Isotherms and Its Reusability. *Chemosphere* **2024**, *354*, 141702. [\[CrossRef\]](#) [\[PubMed\]](#)
25. Silveira Neto, A.L.; Pimentel-Almeida, W.; Niero, G.; Wanderlind, E.H.; Radetski, C.M.; Almerindo, G.I. Application of a Biochar Produced from Malt Bagasse as a Residue of Brewery Industry in Fixed-Bed Column Adsorption of Paracetamol. *Chem. Eng. Res. Des.* **2023**, *194*, 779–786. [\[CrossRef\]](#)
26. Kazak, O.; Akkaya, G.K.; Tor, A. Sustainable and Efficient Removal of Cationic, Anionic and Neutral Dyes from Water by Pre-Deposited Vinasse Biochar Membrane. *J. Environ. Chem. Eng.* **2023**, *11*, 110042. [\[CrossRef\]](#)
27. Chen, W.-H.; Hoang, A.T.; Nižetić, S.; Pandey, A.; Cheng, C.K.; Luque, R.; Ong, H.C.; Thomas, S.; Nguyen, X.P. Biomass-Derived Biochar: From Production to Application in Removing Heavy Metal-Contaminated Water. *Process Saf. Environ. Prot.* **2022**, *160*, 704–733. [\[CrossRef\]](#)
28. Kumar, P.S.; Gayathri, R.; Rath, B.S. A Review on Adsorptive Separation of Toxic Metals from Aquatic System Using Biochar Produced from Agro-Waste. *Chemosphere* **2021**, *285*, 131438. [\[CrossRef\]](#)

29. Qiu, B.; Tao, X.; Wang, H.; Li, W.; Ding, X.; Chu, H. Biochar as a Low-Cost Adsorbent for Aqueous Heavy Metal Removal: A Review. *J. Anal. Appl. Pyrolysis* **2021**, *155*, 105081. [\[CrossRef\]](#)
30. Viotti, P.; Marzeddu, S.; Antonucci, A.; Décima, M.A.; Lovascio, P.; Tatti, F.; Boni, M.R. Biochar as Alternative Material for Heavy Metal Adsorption from Groundwaters: Lab-Scale (Column) Experiment Review. *Materials* **2024**, *17*, 809. [\[CrossRef\]](#)
31. Hama Aziz, K.H.; Kareem, R. Recent Advances in Water Remediation from Toxic Heavy Metals Using Biochar as a Green and Efficient Adsorbent: A Review. *Case Stud. Chem. Environ. Eng.* **2023**, *8*, 100495. [\[CrossRef\]](#)
32. Xiang, W.; Zhang, X.; Chen, J.; Zou, W.; He, F.; Hu, X.; Tsang, D.C.W.; Ok, Y.S.; Gao, B. Biochar Technology in Wastewater Treatment: A Critical Review. *Chemosphere* **2020**, *252*, 126539. [\[CrossRef\]](#)
33. Liang, L.; Xi, F.; Tan, W.; Meng, X.; Hu, B.; Wang, X. Review of Organic and Inorganic Pollutants Removal by Biochar and Biochar-Based Composites. *Biochar* **2021**, *3*, 255–281. [\[CrossRef\]](#)
34. Xiang, L.; Liu, S.; Ye, S.; Yang, H.; Song, B.; Qin, F.; Shen, M.; Tan, C.; Zeng, G.; Tan, X. Potential Hazards of Biochar: The Negative Environmental Impacts of Biochar Applications. *J. Hazard. Mater.* **2021**, *420*, 126611. [\[CrossRef\]](#) [\[PubMed\]](#)
35. Kamali, M.; Appels, L.; Kwon, E.E.; Aminabhavi, T.M.; Dewil, R. Biochar in Water and Wastewater Treatment—A Sustainability Assessment. *Chem. Eng. J.* **2021**, *420*, 129946. [\[CrossRef\]](#)
36. Lu, L.; Yu, W.; Wang, Y.; Zhang, K.; Zhu, X.; Zhang, Y.; Wu, Y.; Ullah, H.; Xiao, X.; Chen, B. Application of Biochar-Based Materials in Environmental Remediation: From Multi-Level Structures to Specific Devices. *Biochar* **2020**, *2*, 1–31. [\[CrossRef\]](#)
37. Mohammadi, R.; Hezarjaribi, M.; Ramasamy, D.L.; Sillanpää, M.; Pihlajamäki, A. Application of a Novel Biochar Adsorbent and Membrane to the Selective Separation of Phosphate from Phosphate-Rich Wastewaters. *Chem. Eng. J.* **2021**, *407*, 126494. [\[CrossRef\]](#)
38. Ghaffar, A.; Zhu, X.; Chen, B. Biochar Composite Membrane for High Performance Pollutant Management: Fabrication, Structural Characteristics and Synergistic Mechanisms. *Environ. Pollut.* **2018**, *233*, 1013–1023. [\[CrossRef\]](#) [\[PubMed\]](#)
39. Zhang, D.; Zhang, K.; Hu, X.; Xue, Y.; Zhang, L.; Sun, Y. Ball-Milled Biochar Incorporated Polydopamine Thin-Film Composite (PDA/TFC) Membrane for High-Flux Separation of Tetracyclic Antibiotics from Wastewater. *Sep. Purif. Technol.* **2021**, *272*, 118957. [\[CrossRef\]](#)
40. He, J.; Song, Y.; Chen, J.P. Development of a Novel Biochar/PSF Mixed Matrix Membrane and Study of Key Parameters in Treatment of Copper and Lead Contaminated Water. *Chemosphere* **2017**, *186*, 1033–1045. [\[CrossRef\]](#)
41. Saad, A.G.; El-Hakam, S.A.; Ahmed, A.I.; Ibrahim, A.A.; Gebreil, A. Highly Salt Resistant Composite Based Protonated G-C3N4@rGO/Biochar for Photocatalytic Degradation of Organic Dyes through Simultaneous Solar Steam-Electricity Generation. *J. Water Process Eng.* **2024**, *58*, 104840. [\[CrossRef\]](#)
42. Wei, Y.; Zhang, Y.; Gao, X.; Ma, Z.; Wang, X.; Gao, C. Multilayered Graphene Oxide Membranes for Water Treatment: A Review. *Carbon* **2018**, *139*, 964–981. [\[CrossRef\]](#)
43. Liu, X.; Ma, R.; Wang, X.; Ma, Y.; Yang, Y.; Zhuang, L.; Zhang, S.; Jehan, R.; Chen, J.; Wang, X. Graphene Oxide-Based Materials for Efficient Removal of Heavy Metal Ions from Aqueous Solution: A Review. *Environ. Pollut.* **2019**, *252*, 62–73. [\[CrossRef\]](#)
44. Liu, H.; Wang, H.; Zhang, X. Facile Fabrication of Freestanding Ultrathin Reduced Graphene Oxide Membranes for Water Purification. *Adv. Mater.* **2015**, *27*, 249–254. [\[CrossRef\]](#) [\[PubMed\]](#)
45. Wang, J.; Chen, B. Adsorption and Coadsorption of Organic Pollutants and a Heavy Metal by Graphene Oxide and Reduced Graphene Materials. *Chem. Eng. J.* **2015**, *281*, 379–388. [\[CrossRef\]](#)
46. Arias Arias, F.; Guevara, M.; Tene, T.; Angamarca, P.; Molina, R.; Valarezo, A.; Salguero, O.; Vacacela Gomez, C.; Arias, M.; Caputi, L.S. The Adsorption of Methylene Blue on Eco-Friendly Reduced Graphene Oxide. *Nanomaterials* **2020**, *10*, 681. [\[CrossRef\]](#) [\[PubMed\]](#)
47. Latorrata, S.; Cristiani, C.; Basso Peressut, A.; Brambilla, L.; Bellotto, M.; Dotelli, G.; Finocchio, E.; Gallo Stampino, P.; Ramis, G. Reduced Graphene Oxide Membranes as Potential Self-Assembling Filter for Wastewater Treatment. *Minerals* **2020**, *11*, 15. [\[CrossRef\]](#)
48. Yu, H.; He, Y.; Xiao, G.; Fan, Y.; Ma, J.; Gao, Y.; Hou, R.; Chen, J. Weak-Reduction Graphene Oxide Membrane for Improving Water Purification Performance. *J. Mater. Sci. Technol.* **2020**, *39*, 106–112. [\[CrossRef\]](#)
49. Yang, K.; Zhu, X.; Chen, B. Facile Fabrication of Freestanding All-Carbon Activated Carbon Membranes for High-Performance and Universal Pollutant Management. *J. Mater. Chem. A* **2017**, *5*, 20316–20326. [\[CrossRef\]](#)
50. Ashraf, A.; Liu, G.; Arif, M.; Mian, M.M.; Rashid, A.; Yousaf, B.; Khawar, M.I.; Riaz, L.; Safeer, R. Insights into the Synthesis and Application of Biochar Assisted Graphene-Based Materials in Antibiotic Remediation. *J. Clean. Prod.* **2022**, *361*, 132211. [\[CrossRef\]](#)
51. Tang, J.; Lv, H.; Gong, Y.; Huang, Y. Preparation and Characterization of a Novel Graphene/Biochar Composite for Aqueous Phenanthrene and Mercury Removal. *Bioresour. Technol.* **2015**, *196*, 355–363. [\[CrossRef\]](#)
52. Carneiro, J.S.D.S.; Leite, D.A.D.C.; Castro, G.M.D.; Franca, J.R.; Botelho, L.; Soares, J.R.; Oliveira, J.E.D.; Melo, L.C.A. Biochar-Graphene Oxide Composite Is Efficient to Adsorb and Deliver Copper and Zinc in Tropical Soil. *J. Clean. Prod.* **2022**, *360*, 132170. [\[CrossRef\]](#)



53. Liu, T.; Gao, B.; Fang, J.; Wang, B.; Cao, X. Biochar-Supported Carbon Nanotube and Graphene Oxide Nanocomposites for Pb(II) and Cd(II) Removal. *RSC Adv.* **2016**, *6*, 24314–24319. [\[CrossRef\]](#)
54. Zhang, Y.; Cao, B.; Zhao, L.; Sun, L.; Gao, Y.; Li, J.; Yang, F. Biochar-Supported Reduced Graphene Oxide Composite for Adsorption and Coadsorption of Atrazine and Lead Ions. *Appl. Surf. Sci.* **2018**, *427*, 147–155. [\[CrossRef\]](#)
55. Roupova, P.; Klouda, K.; Kubatova, H.; Slivkova, S. Preparation and Modification of Hybrid Compounds Based on Go-Biochar and Verification of Their Sorption Properties. *Chem. Eng. Trans.* **2021**, *84*, 61–66. [\[CrossRef\]](#)
56. Xiong, S.; Wu, Z.; Li, Z. Facile Fabrication of Robust, Versatile, and Recyclable Biochar-Graphene Oxide Composite Monoliths for Efficient Removal of Different Contaminants in Water. *Chemosphere* **2022**, *287*, 132418. [\[CrossRef\]](#)
57. Wei, C.; Xiang, C.; Ren, E.; Cui, C.; Zhou, M.; Xiao, H.; Jiang, S.; Yao, G.; Shen, H.; Guo, R. Synthesis of 3D Lotus Biochar/Reduced Graphene Oxide Aerogel as a Green Adsorbent for Cr(VI). *Mater. Chem. Phys.* **2020**, *253*, 123271. [\[CrossRef\]](#)
58. Liang, Y.; Xu, X.; Yuan, F.; Lin, Y.; Xu, Y.; Zhang, Y.; Chen, D.; Wang, W.; Hu, H.; Ou, J.Z. Graphene Oxide Additive-Driven Widening of Microporous Biochar for Promoting Water Pollutant Capturing. *Carbon* **2023**, *205*, 40–53. [\[CrossRef\]](#)
59. Yuan, J.-H.; Xu, R.-K.; Zhang, H. The Forms of Alkalies in the Biochar Produced from Crop Residues at Different Temperatures. *Bioresour. Technol.* **2011**, *102*, 3488–3497. [\[CrossRef\]](#)
60. Cárdenas-Aguiar, E.; Gascó, G.; Lado, M.; Méndez, A.; Paz-Ferreiro, J.; Paz-González, A. New Insights into the Production, Characterization and Potential Uses of Vineyard Pruning Waste Biochars. *Waste Manag.* **2023**, *171*, 452–462. [\[CrossRef\]](#)
61. Rahman, M.A.; Oomori, T. Structure, Crystallization and Mineral Composition of Sclerites in the Alcyonarian Coral. *J. Cryst. Growth* **2008**, *310*, 3528–3534. [\[CrossRef\]](#)
62. Alfattani, R.; Shah, M.A.; Siddiqui, M.I.H.; Ali, M.A.; Alnaser, I.A. Bio-Char Characterization Produced from Walnut Shell Biomass through Slow Pyrolysis: Sustainable for Soil Amendment and an Alternate Bio-Fuel. *Energies* **2021**, *15*, 1. [\[CrossRef\]](#)
63. Lerdkanchanaporn, S.; Dollimore, D.; Alexander, K.S. A Thermogravimetric Study of Ascorbic Acid and Its Excipients in Pharmaceutical Formulations. *Thermochim. Acta* **1996**, *284*, 115–126. [\[CrossRef\]](#)
64. Delgado-Moreno, L.; Bazhari, S.; Gasco, G.; Méndez, A.; El Azzouzi, M.; Romero, E. New Insights into the Efficient Removal of Emerging Contaminants by Biochars and Hydrochars Derived from Olive Oil Wastes. *Sci. Total Environ.* **2021**, *752*, 141838. [\[CrossRef\]](#) [\[PubMed\]](#)
65. Bekiaris, G.; Peltre, C.; Jensen, L.S.; Bruun, S. Using FTIR-Photoacoustic Spectroscopy for Phosphorus Speciation Analysis of Biochars. *Spectrochim. Acta Part A Mol. Biomol. Spectrosc.* **2016**, *168*, 29–36. [\[CrossRef\]](#) [\[PubMed\]](#)
66. Ivanova, N.V.; Korolenko, E.A.; Korolik, E.V.; Zhibankov, R.G. IR Spectrum of Cellulose. *J. Appl. Spectrosc.* **1989**, *51*, 847–851. [\[CrossRef\]](#)
67. De Silva, K.K.H.; Huang, H.-H.; Yoshimura, M. Progress of Reduction of Graphene Oxide by Ascorbic Acid. *Appl. Surf. Sci.* **2018**, *447*, 338–346. [\[CrossRef\]](#)
68. Jabbari, A.; Ghanbari, H.; Naghizadeh, R. Partial Reduction of Graphene Oxide toward the Facile Fabrication of Desalination Membrane. *Int. J. Environ. Sci. Technol.* **2023**, *20*, 831–842. [\[CrossRef\]](#)
69. Jiang, S.; Huang, L.; Nguyen, T.A.H.; Ok, Y.S.; Rudolph, V.; Yang, H.; Zhang, D. Copper and Zinc Adsorption by Softwood and Hardwood Biochars under Elevated Sulphate-Induced Salinity and Acidic pH Conditions. *Chemosphere* **2016**, *142*, 64–71. [\[CrossRef\]](#)
70. Chen, X.; Chen, G.; Chen, L.; Chen, Y.; Lehmann, J.; McBride, M.B.; Hay, A.G. Adsorption of Copper and Zinc by Biochars Produced from Pyrolysis of Hardwood and Corn Straw in Aqueous Solution. *Bioresour. Technol.* **2011**, *102*, 8877–8884. [\[CrossRef\]](#)
71. Kumar, A.; Kumar, K.; Kaur, K.; Arya, K.; Mehta, S.K.; Singh, S.; Kataria, R. Zn-MOF@rGO Nanocomposite: A Versatile Tool for Highly Selective and Sensitive Detection of Pb<sup>2+</sup> and Cu<sup>2+</sup> Ions in Water. *Anal. Methods J.* **2024**, *16*, 6020–6029. [\[CrossRef\]](#)
72. Xi, Y.-H.; Hu, J.-Q.; Liu, Z.; Xie, R.; Ju, X.-J.; Wang, W.; Chu, L.-Y. Graphene Oxide Membranes with Strong Stability in Aqueous Solutions and Controllable Lamellar Spacing. *ACS Appl. Mater. Interfaces J.* **2016**, *8*, 15557–15566. [\[CrossRef\]](#)
73. Yuan, W.; Li, C.; Chu, T.; Cheng, M.; Hou, S. In-Situ Chemical Formation of Strong Stability GO/rGO Hybrid Membranes for Efficient Treatment of Organic Pollutant. *Mater. Lett.* **2022**, *314*, 131849. [\[CrossRef\]](#)
74. Li, C.; Li, Z.; Wang, Z.; Guan, K.; Chiao, Y.-H.; Zhang, P.; Xu, P.; Gonzales, R.R.; Hu, M.; Mai, Z.; et al. Fabrication of Polydopamine/rGO Membranes for Effective Radionuclide Removal. *ACS Omega* **2024**, *9*, 14187–14197. [\[CrossRef\]](#) [\[PubMed\]](#)
75. Thebo, K.H.; Qian, X.; Zhang, Q.; Chen, L.; Cheng, H.-M.; Ren, W. Highly Stable Graphene-Oxide-Based Membranes with Superior Permeability. *Nat. Commun.* **2018**, *9*, 1486. [\[CrossRef\]](#) [\[PubMed\]](#)
76. Yaashikaa, P.R.; Kumar, P.S.; Varjani, S.; Saravanan, A. A Critical Review on the Biochar Production Techniques, Characterization, Stability and Applications for Circular Bioeconomy. *Biotechnol. Rep.* **2020**, *28*, e00570. [\[CrossRef\]](#)
77. Tomczyk, A.; Sokołowska, Z.; Boguta, P. Biochar Physicochemical Properties: Pyrolysis Temperature and Feedstock Kind Effects. *Rev. Environ. Sci. Biotechnol.* **2020**, *19*, 191–215. [\[CrossRef\]](#)
78. Priyadarsini, A.; Mohanty, C.; Nanda, S.; Mishra, A.; Das, N.; Swain, N.; Dash, M.; Jena, P.K. Synergistic Cobalt Oxide/Reduced Graphene Oxide/Biochar Nano-Composite Catalyst: Harnessing the Power of the Catalyst for Sustainable Remediation of Organic Dyes and Chromium(VI). *RSC Adv.* **2024**, *14*, 10089–10103. [\[CrossRef\]](#)

79. Van Hien, N.; Valsami-Jones, E.; Vinh, N.C.; Phu, T.T.; Tam, N.T.T.; Lynch, I. Effectiveness of Different Biochar in Aqueous Zinc Removal: Correlation with Physicochemical Characteristics. *Bioresour. Technol. Rep.* **2020**, *11*, 100466. [[CrossRef](#)]
80. Kołodziejka, D.; Wnętrzak, R.; Leahy, J.J.; Hayes, M.H.B.; Kwapiński, W.; Hubicki, Z. Kinetic and Adsorptive Characterization of Biochar in Metal Ions Removal. *Chem. Eng. J.* **2012**, *197*, 295–305. [[CrossRef](#)]
81. Dellinger, B.; Lomnicki, S.; Khachatryan, L.; Maskos, Z.; Hall, R.W.; Adounkpe, J.; McFerrin, C.; Truong, H. Formation and Stabilization of Persistent Free Radicals. *Proc. Combust. Inst.* **2007**, *31*, 521–528. [[CrossRef](#)]
82. Dela Cruz, A.L.N.; Gehling, W.; Lomnicki, S.; Cook, R.; Dellinger, B. Detection of Environmentally Persistent Free Radicals at a Superfund Wood Treating Site. *Environ. Sci. Technol.* **2011**, *45*, 6356–6365. [[CrossRef](#)]
83. Godiksen, A.; Stappen, F.N.; Vennestrom, P.N.R.; Giordanino, F.; Rasmussen, S.B.; Lundegaard, L.F.; Mossin, S. Coordination Environment of Copper Sites in Cu-CHA Zeolite Investigated by Electron Paramagnetic Resonance. *J. Phys. Chem. C* **2014**, *118*, 23126–23138. [[CrossRef](#)]
84. Boas, J.F.; Dunhill, R.H.; Pilbrow, J.R.; Srivastava, R.C.; Smith, T.D. Electron Spin Resonance Studies of Copper(II) Hydroxy-Carboxylic Acid Chelates in Aqueous and Non-Aqueous Solutions. *J. Chem. Soc. A* **1969**, 94–108. [[CrossRef](#)]
85. Puglia, M.; Giuliani, M.; Morselli, N.; Ottani, F.; Allesina, G.; Pedrazzi, S.; Tartarini, P. Experimental Investigation of Chestnut Shells Gasification. *J. Phys. Conf. Ser.* **2023**, *2648*, 012017. [[CrossRef](#)]
86. Basso Peressut, A.; Cristiani, C.; Dotelli, G.; Dotti, A.; Latorrata, S.; Bahamonde, A.; Gascó, A.; Hermosilla, D.; Balzarotti, R. Reduced Graphene Oxide/Waste-Derived TiO<sub>2</sub> Composite Membranes: Preliminary Study of a New Material for Hybrid Wastewater Treatment. *Nanomaterials* **2023**, *13*, 1043. [[CrossRef](#)] [[PubMed](#)]
87. Klank, D.; Goverde, T.; Blum, C. *Particle World*; Technical Papers of Quantachrome; Quantachrome: Klundert, The Netherlands, 2009. Available online: [www.quantachrome.com](http://www.quantachrome.com) (accessed on 10 January 2025).

**Disclaimer/Publisher’s Note:** The statements, opinions and data contained in all publications are solely those of the individual author(s) and contributor(s) and not of MDPI and/or the editor(s). MDPI and/or the editor(s) disclaim responsibility for any injury to people or property resulting from any ideas, methods, instructions or products referred to in the content.